

Effect of film thickness on the solar cell performance of CBD grown CdS/PbS heterostructure

N. Kavitha¹ · R. Chandramohan² · S. Valanarasu³ · T. A. Vijayan² · S. Rex Rosario³ · A. Kathalingam⁴

Received: 12 August 2015 / Accepted: 8 November 2015 / Published online: 14 November 2015
© Springer Science+Business Media New York 2015

Abstract CdS, PbS and CdS/PbS thin films were deposited onto glass and ITO substrates using chemical bath technique. The thickness of the CdS was varied by varying the deposition time and the influence of film thickness on structural, morphological, optical and electrical properties of the as-deposited films were investigated by XRD, SEM, UV–Vis–NIR spectroscopy and two-probe techniques. XRD analysis of CdS and PbS films have shown polycrystalline nature of the films with preferred orientation along (002) and (200) reflections. The grain size of the CdS film was found to increase with the film thickness. Scanning electron microscopic results of the CdS films have revealed smooth morphology and it has found to show increased particle size with the film thickness. Optical transmittance of the CdS thin films was found to decrease with the film thickness. The increase of deposition time is found to shift the band gap from 2.75 to 2.66 eV. Band gap of the PbS film is found to be 1.57 eV for a thickness of 0.89 μm . The photo-response studies done for CdS/PbS heterojunction solar cells have indicated that the film thickness has an influence on the cell efficiency. The observed enhancement in solar cell properties is attributed

to the changes in the morphology, the crystalline quality and the optical properties caused by the increase of film thickness.

1 Introduction

Polycrystalline CdS thin films have been received considerable attention considering its use in photovoltaic, electroluminescent [1, 2] and field effect transistors [3]. It has been used as a partner in several types of thin film solar cells, such as, CuInSe₂, CdTe and Cu₂S [4–6]. CdS is a most promising heterojunction partner for the well-known polycrystalline photovoltaic material as a window layer [7]. Hernandez-Borja et al. [8] fabricated CdS/PbSe solar cell with CdS window layer. Nair et al. [9] prepared CdS as window layer for CdS/PbS solar cell. For solar cell applications the grown films of CdS should have suitable conductivity ($>10^{16}$ carriers/cm³), and adequate thickness to allow high transmission and also it should be highly uniform without voids and holes to avoid electrical short circuit effects. To get desired property of the films, the growth methods and the growth conditions should be chosen accordingly. Getting films of particular properties depends on the deposition method and the conditions of preparation. CdS thin films can be prepared by chemical, physical and electrochemical methods. It has been grown by variety of methods such as vacuum evaporation [10], molecular beam epitaxy [11], sputtering [12], spray pyrolysis [13], electrochemical deposition [14], pulsed laser deposition [15], metal organic chemical vapour deposition [16], successive ionic layer adsorption and reaction [17] and chemical bath deposition [18] (CBD). The chemical bath deposition method is the most inexpensive method allowing large area fabrication of variety of films; it is a suitable method for

✉ S. Valanarasu
valanroyal@gmail.com

¹ Department of Physics, Vickram College of Engineering, Enathi 630 56, India

² Department of Physics, Sree Sevugan Annamalai College, Devakottai 630303, India

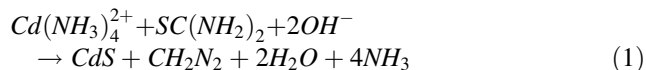
³ PG and Research Department of Physics, Arul Anandar College, Karumathur 625514, India

⁴ Millimeter-Wave Innovation Technology Research Center (MINT), Dongguk University, Seoul 100-715, Republic of Korea

industrial applications. Comparing other methods, the CBD method has many advantages such as simplicity, no requirement of sophisticated instruments, minimum material wastage, economical way of large area deposition, and no need of handling poisonous gases [19]. As it is a slow process, it facilitates better orientated growth with improved grain structures. Chemical bath deposition method also allows easy control of growth parameters, so that good quality and uniform films can be grown to produce desired properties. In photovoltaic applications, the thickness of the film is an important parameter since the thickness affects the microstructure of the film as well as the optical and electrical characteristics. They are only very few data available on the fabrication of PbS/CdS heterojunction solar cells. Hence, an attempt has been made to prepare CdS thin films of different thickness on glass substrates using chemical bath at different deposition times. The prepared CdS and PbS films are studied for their structural, microstructural and optical properties. PbS/CdS heterojunction solar cells were fabricated using CdS film films of different thickness and studied their photo response performance.

2 Experiment procedure

In this work, 0.005 mol/L of CdCl_2 and NH_4Cl were dissolved in 100 mL DI water at room temperature. When heating the solution at 70 °C a 0.04 mol/L of ammonia solution was added and stirred for 5 min and finally 0.03 mol/L of thiourea was added to the solution. The cleaned glass substrates were placed vertically in the reaction bath for different time period such as 30, 45 and 60 min. After the set period the substrates were removed and cleaned with DI water. In the bath, the added ammonia combines with Cd^{2+} and forms $\text{Cd}(\text{NH}_3)_4^{2+}$ complex which can constantly release Cd^{2+} , thiourea releases S^{2-} as a sulfur source. The main chemical reaction taking place in the reaction solution is described in the Eq. (1).



For the preparation of solar cells the PbS thin film was deposited on CdS coated ITO substrates (sheet resistance of ITO is 10 Ω/sq). A 50 ml solution of 0.15 M lead nitrate [$\text{Pb}(\text{NO}_3)_2$] and 0.1 M thiourea [$\text{SC}(\text{NH}_2)_2$] was used for the deposition of PbS. The alkalinity of the solution was set using 0.5 M sodium hydroxide [NaOH]. The CdS coated ITO substrate was vertically immersed into the solution and the beaker containing the reactive solution was kept in a water bath maintained at 60 °C. Thickness of the films was measured using Alpha-step surface profiler and also they were characterized using XRD, SEM, optical absorption and electrical studies. X-ray diffraction pattern

of the films were obtained using X'pert PRO (PANalytical) diffractometer with $\text{CuK}\alpha$ radiation ($k = 0.15405 \text{ nm}$) in steps of 0.1 over the 2θ range of 10°–80°. Morphological examination of the films was done using Hitachi (S-3000H) scanning electron microscope. In order to determine the band gap energy of the films, optical transmission study was carried using Perkin Elmer Lambda 35 spectrophotometer. Photocurrent–voltage measurements were performed using (Keithley 4200 semiconductor parameter analyzer under AM 1.5G illumination at 100 mW/cm^2).

3 Results and discussion

3.1 Structural studies

Figure 1 shows the X-ray diffraction patterns of three CdS films prepared at deposition times 30, 45 and 60 min and PbS film at 120 min. The diffraction peak observed at 26.5° corresponds to (002) plane which is parallel to the substrate surface, this direction is more favorable due to its lowest surface free energy [20]. It is found that the CdS thin films are in hexagonal crystal structure, which is in agreement with standard pattern (JCPDS card no. 41-1049). The crystallinity of the PbS film is also found good and it has shown three characteristics peaks corresponding to (1 1 1), (2 0 0) and (2 2 0) orientations, it is also in good agreement with its standard JCPDS card No. 00-0050592 with cubic rock salt (NaCl) type structure. The narrow peaks observed for CdS indicates that the material has good crystallinity with prepared orientation along the (2 0 0) direction which is perpendicular to the substrate.

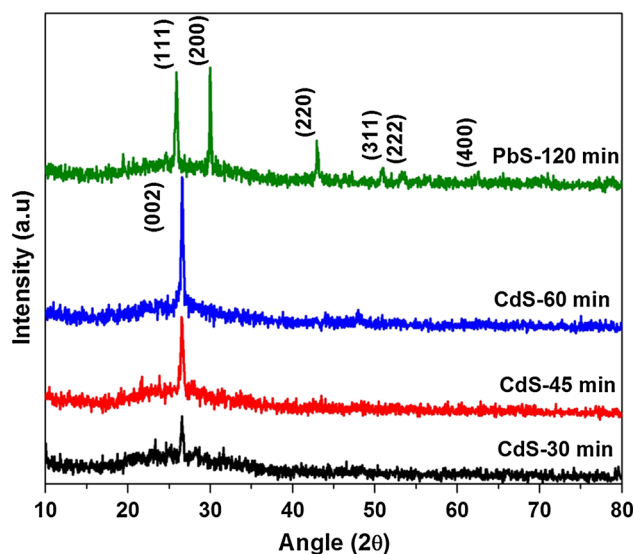


Fig. 1 XRD patterns of CdS and PbS thin films

The average value of the crystallite size was estimated applying the Debye–Scherrer's equation (2).

$$D = \frac{0.9\lambda}{\beta \cos \theta} \quad (2)$$

where, $\lambda = 1.5406 \text{ \AA}$ for $CuK\alpha$, β is the full width at half maximum (FWHM) of the peak and θ is the diffraction Bragg's angle. The calculated crystallite size and other parameters of the films CdS and PbS are shown in Table 1. From the calculated values of crystallite size, the dislocation density and microstrain for all the samples were determined using Eqs. (3) and (4) and the results are also given in Table 1.

$$\delta = \frac{1}{D^2} \quad (3)$$

$$\varepsilon = \frac{\beta \cos \theta}{4} \quad (4)$$

The relation connecting stacking fault probability (α) with peak shift $\Delta(2\theta)$ is given by Warren and Warekois [21] as shown in the Eq. (4).

$$\alpha = \left[\frac{2\pi^2}{45\sqrt{3}} \right] \left[\frac{\Delta(2\theta)}{\tan \theta_{311}} \right] \quad (5)$$

Using the expression (5) the stacking fault probability was calculated by measuring the peak shift with the standard value. The intensity of the prominent peak (002) is found to increase with a reduction in peak broadening as the thickness increases. This indicates that there is an enhancement in crystallite size, reduction of stress and strain in the thin films with increase of film thickness (Table 1). Structural parameters of the PbS thin film also calculated and shown in Table 1. As the CdS film thickness increases, the reduction in microstrain and dislocation density may lead to the relaxation of the stress in the films. This relaxation produces misfit between the substrate and the film as the thickness increases and hence the stacking fault decreases as given in the Table 1. The increase in crystallite size with film thickness is a normal phenomenon it has been reported [22, 23]. Similar effect on the microstrain, dislocation density, and stacking fault probability has also been reported in thin films [24, 25].

3.2 Morphological studies

Figure 2a–c shows SEM image of as-deposited cadmium sulphide thin films deposited for 30, 45 and 60 min respectively. It shows that the substrate is well covered with the deposited material without cracks and holes. And also it reveals that the film formed is smooth and dense. Comparing the SEM images of the films grown at different times, it clearly shows that the grains sizes of the films are increased as deposition time increases. The SEM image shown in Fig. 2d shows surface of the PbS film grown on CdS, it has shown spherical nano grains coated over the CdS. The elemental analysis of CdS–PbS thin films deposited on ITO substrate was performed using EDS analysis and it is presented in Fig. 2e. This EDS spectrum shows the trace Cd, Pb and S confirming the growth of CdS and PbS.

3.3 Optical studies

UV–Vis–NIR spectroscopy helps to study optical behavior and crystallite size of materials. The optical transmittance spectra of CdS films deposited onto a glass substrate were studied at room temperature in the wavelength range of 300–1100 nm. Figure 3 shows the plot of transmittance of CdS thin film as a function of wavelength. All nano films are observed as highly transparent with an average optical transparency (%T) of >50 % in the visible region of solar spectrum. The transmission of the light through the material depends upon the extent of absorption and scattering. There is a decrease of transmittance for the increase in thickness. An increase in film thickness offers a dense structure with improved crystallinity. Hence, high absorption and scattering of light due to increased thickness causes decrease in %T [26, 27]. The absorption coefficient (α) signifying the inter-band transition near the band gap can be obtained from the transmittance (T) values using the Lambert law

$$\alpha = \frac{\ln(1/T)}{t} \quad (6)$$

where t , and T are film thickness and transmittance respectively. The value of α decreases with increase in

Table 1 Thickness and structural parameters of CdS and PbS thin films

Sample	Deposition time (min)	Thickness (μm)	Crystallite size (nm)	Microstrain (ε) lines m^{-2}	Dislocation density (δ)	Stacking fault probability (α) $\times 10^{-4}$
CdS	30	0.42	16	0.00943	3.894	5.6
	45	0.59	17	0.00887	3.449	3.7
	60	0.67	28	0.00532	1.243	3.5
PbS	120	0.89	51	0.00261	0.377	1.4

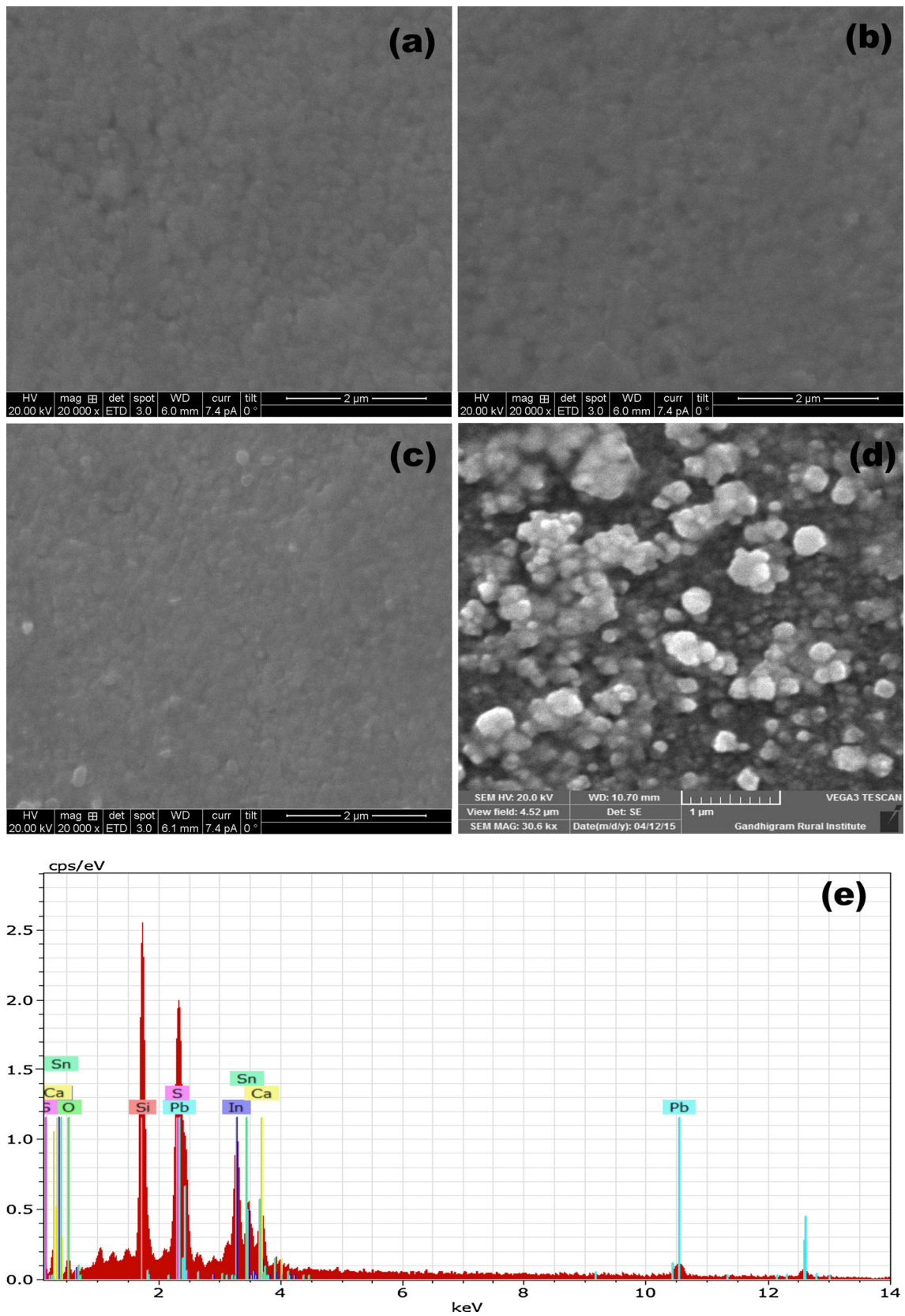


Fig. 2 SEM images of CdS thin films **a** 30 s, **b** 45 s, **c** 60 s, **d** ITO/CdS/PbS structure and **e** EDAX image of solar cell

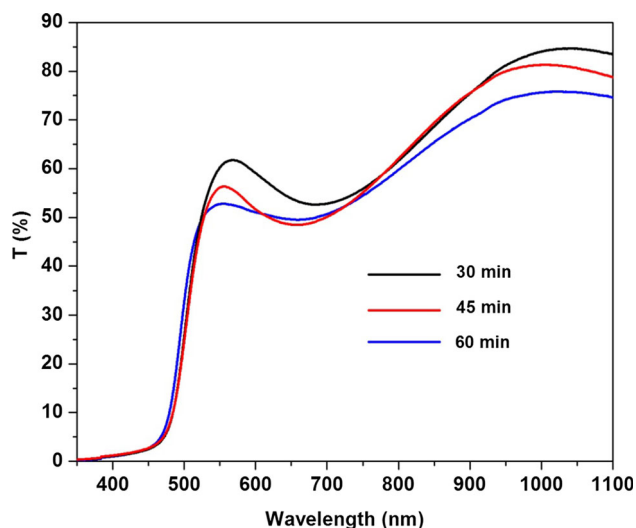


Fig. 3 Optical transmission spectra of CdS thin films

thickness of the deposited films in the band to band absorption region as observed elsewhere [28, 29]. The relatively high values of α ($\sim 10^5 \text{ cm}^{-1}$) at fundamental absorption edge may be due to increase in crystallite size (Table 1) and increase in light absorption (Fig. 3). In all nano films under investigation, a shift in absorption edge towards higher wavelengths for the increase in film thickness has been observed. The following relation was used to calculate the optical band gap with direct transitions of the CdS film,

$$(\alpha h\nu) = B(h\nu - E_g)^{1/2} \quad (7)$$

where $h\nu$ is the photon energy, α is the absorption coefficient, E_g is the optical band gap and B is a constant. For calculation of the optical band gap of CdS film, the curve of $(\alpha h\nu)^2$ versus $h\nu$ was plotted. The E_g values of CdS film determined from the Fig. 4 are found to be 2.75–2.66 eV, which are higher than the reported values [30]. The value of E_g decreases with increase in thickness (Table 2). This may be due to increase in crystallite size, decrease in stacking faults and crystal imperfection (Table 1) which results in orientation of the crystallites and defect-free grain boundaries. The high value of E_g in the nano films in comparison to bulk CdS may be attributed to the quantum confinement associated with the existence of nano crystallites in the semiconductor material and the low-dimensional film structure. The Fig. 5 shows the transmittance of PbS film, and the band gap determined for this film is found to be 1.57 eV (Fig. 6).

3.4 Photoresponse I–V characteristics

The photocurrent–voltage (I–V) performances of the ITO/CdS/PbS/Al solar cells are shown in Fig. 7. The open-circuit voltage (V_{oc}) is found to increase from 0.33 to

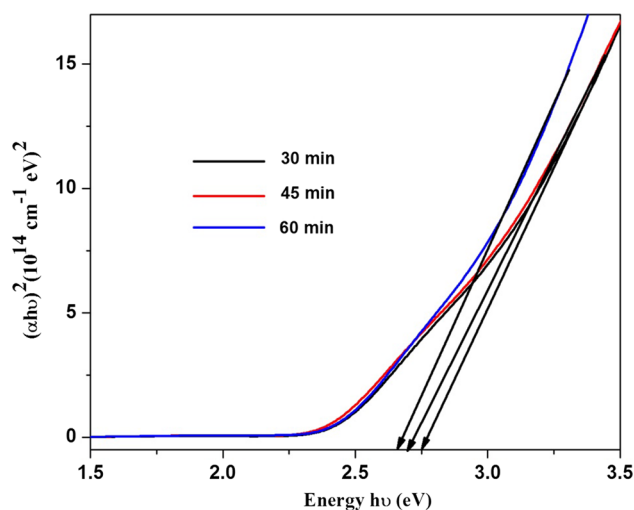


Fig. 4 Plot of $(\alpha h\nu)^2$ ($\text{eV}^2 \text{ cm}^{-2}$) versus photon energy (eV) of CdS thin films

0.37 V and the short circuit current density (J_{sc}) is increased from 6.23 to 6.69 mA/cm^2 with the increase of thickness. These results revealed that the increase of deposition time increases the open-circuit voltage, which may be due to the decrease in energy band gap of the films.

The fill factor (FF) was calculated using the following relationship:

$$FF = \frac{(J_{sc} V_{oc})_{\max}}{J_{sc} \times V_{oc}} \quad (8)$$

The energy conversion efficiency (η) can therefore be calculated using the equation:

$$\eta = \frac{FF \times J_{sc} \times V_{oc}}{P_{in}} \quad (9)$$

The efficiency of the solar cells was estimated to be 0.782, 0.891 and 1.11 % respectively for the deposition time of 30, 45 and 60 min, respectively. It was lower than Obaid et al. [31] and Borja et al. [32] fabricated solar cells using PbS/CdS. The results obtained in this work show that the efficiency of the cell can be increased by increasing the thickness of the films due to increased deposition time. The series resistance (R_s) and shunt resistance (R_{sh}) of all the three samples were estimated using Eqs. (10) and (11), respectively

$$\left[\frac{dI}{dV} \right]_{I=0} \cong \frac{1}{R_s} \quad (10)$$

$$\left[\frac{dI}{dV} \right]_{V=0} \cong \frac{1}{R_{sh}} \quad (11)$$

A low series resistance can permit high current through the cell at low applied voltages. This series resistance is obtained due to contact resistance and bulk resistance of the photoactive material.

Table 2 Device parameters of all solar cells tested at the room temperature

CdS deposition time (s)	V_{oc} (V)	I_{sc} (mA)	FF (%)	Efficiency (%)	R_s (Ωcm^2)	R_{sh} (Ωcm^2)
30	0.33	6.23	38.03	0.78	27	128
45	0.34	6.45	40.59	0.89	23	277
60	0.37	6.69	44.81	1.11	21	533

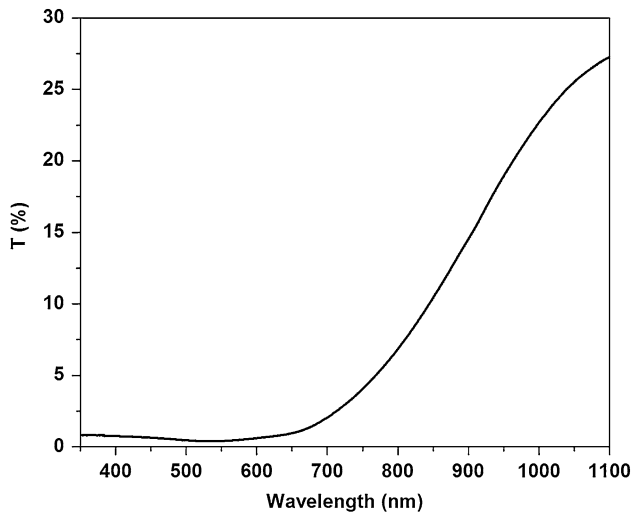


Fig. 5 Optical transmission spectra of PbS thin films

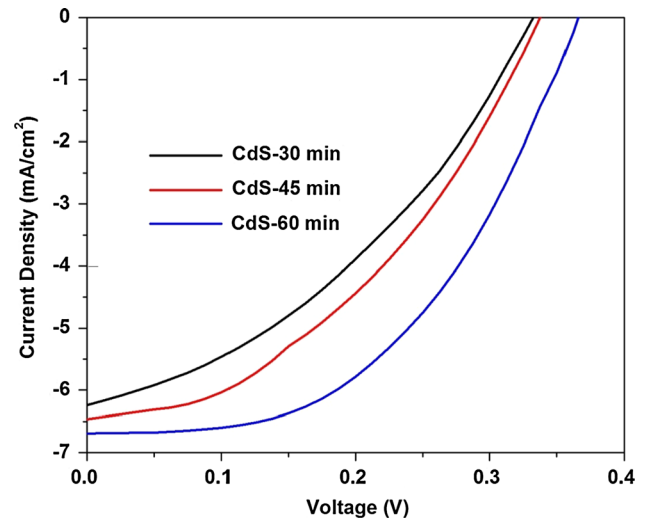


Fig. 7 I–V curves for the solar cells ITO/CdS/PbS/Al cell

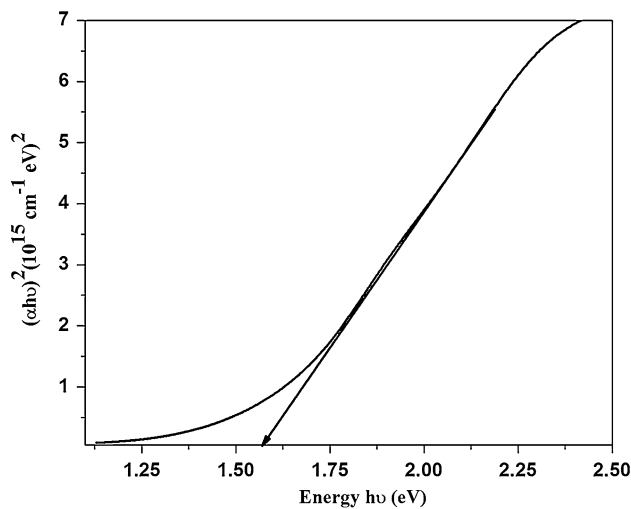


Fig. 6 Plot of $(\alpha h\nu)^2$ ($\text{eV}^2 \text{cm}^{-2}$) versus photon energy (eV) of PbS thin films

A large shunt resistance is resulted if there are shorts or leaks of photocurrent in the device. Detailed parameters of the solar cells extracted from the I–V characteristics are listed in Table 2. This significant improvement in photovoltaic performance of the fabricated ITO/CdS/PbS/Al solar cells may be attributed to the following reasons: (1) An enhanced absorption of sunlight caused by the red shift of the bandgap resulting enhanced current density. (2) The

increased grain size can reduce the particle-to-particle hopping of the photo-induced carrier. (3) The improvement in the quality of the CdS thin films without imperfections and defects, which may reduce the recombination of photo-excited carriers resulting high power conversion efficiency. The results obtained in this study have shown an improvement comparing the earlier reports [33, 34].

4 Conclusion

CdS, PbS and CdS/PbS thin films were successfully grown on glass and ITO coated glass substrates. The CdS thin films have shown hexagonal phase with a preferred orientation in the (0 0 2) plane. PbS film has shown cubic rock salt structure with (200) preferred orientation. SEM analysis of the films has shown uniformly distribution of grains on the substrate. The grain size and thickness of the films was found to increase with the deposition time. Optical characterization has done for the films have shown decrease of band gap with the increase of deposition time. The conversion efficiency of the fabricated solar cells is found increase from 0.78 up to 1.1 %, as CdS deposition time increases. This improvement can be associated with several factors, but mostly attributed to the enhancement of crystallinity. It is found that the deposition time has a significant effect on solar efficiency.

Acknowledgments The author has gratefully acknowledged the UGC-No. F.41-913/2012 (SR), India for providing financial support to carry out this work.

References

1. A. Gokarna, N.R. Pavaskar, S.D. Sathaye, V. Ganesan, S.V. Bhoraskar, *J. Appl. Phys.* **92**, 2118 (2002)
2. Y. Kashiwaba, J. Sato, T. Abe, *Appl. Surf. Sci.* **212**, 162 (2003)
3. C. Voss, S. Subramanian, C.H. Chang, *J. Appl. Phys.* **96**, 5819 (2004)
4. J.H. Wi, W.J. Lee, D.H. Cho, W.S. Han, J.H. Yun, Y.D. Chung, *Phys. Status Solidi (a)* **211**, 2172 (2014)
5. S. Girish Kumar, K.S.R. Koteswara Rao, *Energy Environ. Sci.* **7**, 45–102 (2014)
6. C. Pan, S. Niu, Y. Ding, L. Dong, R. Yu, Y. Liu, G. Zhu, Z. Lin Wang, *Nano Lett.* **12**, 3302–3307 (2012)
7. J.N. Ximello-Quiebras, G. Contreras-Puente, J. Aguilar Hernandez, G. Santana-Rodriguez, A. Arias-Carbajal Readigos, *Sol. Energy Mater. Sol. Cells* **82**, 263e8 (2004)
8. J. Hernández-Borja, Y.V. Vorobiev, R. Ramirez-Bon, *Sol. Energy Mater. Sol. Cells* **95**, 1882e8 (2011)
9. P.K. Nair, E. Barrios-Salgado, J. Capistran, M.L. Ramon, M.T.S. Nair, R.A. Zingaro, *J. Electrochem. Soc.* **157**, D528e37 (2010)
10. S.A. Mahmoud, A.A. Ibrahim, A.S. Riad, *Thin Solid Films* **372**, 144 (2000)
11. J.W. Choi, A. Bhupathiraju, M.A. Hasan, M. John Lannon, *J. Cryst. Growth* **255**, 1 (2003)
12. N. Romeo, A. Bosio, R. Tedeschi, A. Romeo, V. Canevari, *Sol. Energy Mater. Sol. Cells* **58**, 209 (1999)
13. S.A. Yuksel, S. Gunes, Y. Guney, *Thin Solid Films* **540**, 242 (2013)
14. G. Sasikala, R. Dhanasekaran, C. Subramanian, *Thin Solid Films* **302**, 71 (1997)
15. B. Ullrich, H. Sakai, Y. Segawa, *Thin Solid Films* **385**, 220 (2001)
16. H. Uda, H. Yonezawa, Y. Ohtsubo, M. Kosaka, H. Sonomura, *Sol. Energy Mater. Sol. Cells* **75**, 219 (2003)
17. C.D. Lokhande, B.R. Sankapal, H.M. Pathan, M. Muller, M. Giersig, H. Tributsch, *Appl. Surf. Sci.* **18**, 277 (2001)
18. H. Moualkia, S. Hariech, M.S. Aida, N. Attaf, E.L. Lifa, *J. Phys. D Appl. Phys.* **42**, 135404 (2009)
19. M. Dhanam, R. Balasundraprabhu, S. Jayakumar, P. Gopalakrishnan, M.D. Kannan, *Phys. Status Solidi (a)* **191**, 149 (2002)
20. C.D.G. Lazos, E. Rosendo, B.H. Juarez, G.G. Salgado, T. Diaz, M.R. Falfan, A.I. Oliva, P. Quintana, D.H. Aguilar, W. Cauich, M. Ortega, Y. Matsumoto, *J. Electrochem. Soc.* **155**, D158 (2008)
21. B.E. Warren, E.P. Warekoi, *Acta Metall.* **3**, 473 (1995)
22. H. Kim, J.S. Horwitz, G. Kushto, A. Pique, Z.H. Kafafi, C.M. Gilmore, D.B. Chrisey, *J. Appl. Phys.* **88**, 6021 (2000)
23. S. Lalitha, R. Sathyamoorthy, S. Senthilarasu, A. Subbarayan, K. Natarajan, *Sol. Energy Mater. Sol. Cells* **82**, 187 (2004)
24. U. Pal, D. Samanta, S. Ghorai, B.K. Samantaray, A.K. Chaudhuri, *J. Phys. D Appl. Phys.* **25**, 1488 (1992)
25. H.L. Chen, Y.M. Lu, W.S. Hwang, *JIM Mater. Trans.* **46**, 872 (2005)
26. S. Kumar, P. Sharma, V. Sharma, *J. Appl. Phys.* **111**, 043519 (2012)
27. J.H. Lee, W.C. Song, J.S. Yi, K.J. Yang, W.D. Han, J. Hwang, *Thin Solid Films* **431**, 349 (2003)
28. H. Metin, R. Esen, *Semicond. Sci. Technol.* **18**, 647 (2003)
29. E. Cetinorgu, C. Gumus, R. Esen, *Thin Solid Films* **515**, 1688 (2006)
30. M.A. Islam, M.S. Hossain, M.M. Aliyu, P. Chelvanathan, Q. Huda, M.R. Karim, K. Sopian, N. Amin, *Energy Procedia* **33**, 203 (2013)
31. A.S. Obaid, M.A. Mahdi, Z. Hassan, M. Bououdin, *Int. J. Hydrog. Energy* **38**, 807 (2013)
32. J.H. Borja, Y.V. Vorobiev, R.R. Bon, *Sol. Energy Mater. Sol. Cells* **95**, 1882 (2011)
33. H. Moreno-Garcia, M.T.S. Nair, P.K. Nair, *Thin Solid Films* **519**, 7364e8 (2011)
34. M.A. Barote, A.A. Yadav, T.V. Chavanan, E.U. Masumdar, *Dig. J. Nanomater. Biostruct.* **6**, 979e90 (2011)